

# Criticality of a classical dimer model on the triangular lattice

F. Trouselet, P. Pujol, F. Alet and D. Poilblanc

*Laboratoire de Physique Théorique, CNRS, Université Paul Sabatier, 31062 Toulouse, France.*

(Dated: January 13, 2022)

We consider a classical interacting dimer model which interpolates between the square lattice case and the triangular lattice case by tuning a chemical potential in the diagonal bonds. The interaction energy simply corresponds to the number of plaquettes with parallel dimers. Using transfer matrix calculations, we find in the anisotropic triangular case a succession of different physical phases as the interaction strength is increased: a short range disordered liquid dimer phase at low interactions, then a critical phase similar to the one found for the square lattice, and finally a transition to an ordered columnar phase for large interactions. The existence of the critical phase is in contrast with the belief that criticality for dimer models is ascribed to bipartiteness. For the isotropic triangular case, we have indications that the system undergoes a first order phase transition to an ordered phase, without appearance of an intermediate critical phase.

## I. INTRODUCTION

Dimer models have regained a lot of interest in the condensed matter physics community thanks to the pioneering work of Rokhsar and Kivelson (RK) [1]. In this original proposal, dimers represent singlets formed by pairs of spins  $1/2$  in Cuprate materials or frustrated antiferromagnetic systems. This idea has been followed by many other proposals giving rise, at low energy, to such kind of effective models. To cite only a few connections to the physics of dimers, related again to magnetism, the lowest-energy configurations of fully frustrated Ising magnets can generally be mapped onto dimer configurations on the dual lattice [2, 3]. Other specific (quantum) dimer models have recently been derived from a spin-orbital model describing  $\text{LiNiO}_2$  [4], from the trimerized *kagome* antiferromagnet [5], or for Heisenberg antiferromagnets under applied field in the pyrochlore lattice [6]. Lastly, we note that hard-core bosons or correlated fermions on frustrated lattices like the planar pyrochlore lattice can also be mapped onto dimer representations in the limit of large Coulomb repulsion [7, 8].

Although the RK model is quantum mechanical, there is a special value of the parameters of the Hamiltonian for which the ground-state is an equal weight superposition of all dimer tilings of the square lattice (RK point). Static properties at zero temperature can then be understood by the purely combinatorial problem of counting dimer tilings of the square lattice first solved in the early 60's [9]. This system turns out to be a critical model, and more precisely a conformal field theory with central charge  $c = 1$ . Subsequently to the RK work, Moessner and Sondhi [10] have shown that the same dimer model on the triangular lattice shows, instead of a single point with critical algebraic correlations, a disordered phase with short range dimer correlations - as expected from the known physics of its classical counterpart [11]. From the interpretation originally given to the dimers, it is legitimate to call this phase a spin liquid.

More recently, a study performed by Alet *et al.* [12] on a square lattice classical dimer model showed the existence of a Kosterlitz-Thouless phase transition from a

critical phase to a columnar ordered phase for the dimers. This transition is triggered by including an interaction term, consisting in the number of plaquettes doubly occupied by parallel dimers. Subsequently, a quantum mechanical dimer model can be built from this classical model proving that the single point showing criticality in the original RK Hamiltonian can be promoted to a whole critical phase [13].

An important difference between the square and the triangular lattices for quantum dimer models lies in the degeneracy of the ground state at the RK point: it is finite for the triangular lattice with periodic boundary conditions (PBC) and scales exponentially with the linear size for the square lattice with the same PBC (see Ref. 10 and Ref. 1 respectively for details). This large degeneracy of the square lattice, related to its bipartiteness, has been often designated as the responsible of the existence of critical correlations in this case. It is then natural to investigate the behavior of interacting dimer model on non-bipartite lattices interpolating between the square and the triangular lattices, and in particular try to elucidate the interplay between criticality and bipartiteness. In the non-interacting case, it is found [11] that criticality disappears immediately with the introduction of non-bipartite dimers.

In this paper we study an extension of the classical dimer model with nearest-neighbor interactions already studied elsewhere [12, 13] to the case of an anisotropic triangular lattice. Although a limiting case of this model is the square lattice, in general the lattice is non-bipartite. In Sec. II we start by reviewing the results on the square lattice, and recalling the principles of an associated field theory used to describe the critical phase. In Sec. III, we investigate the properties of the anisotropic model that interpolates between the square and triangular lattices by means of transfer matrix calculations. There are two independent paths for the interpolation: the introduction of a fugacity for *diagonal* bonds but also of the introduction of interactions between parallel dimers on *diamond-like* plaquettes (see Fig. 1). We find for a certain range of parameters the existence of a critical phase. We determine its location in the phase diagram as well

as transitions from it to either liquid or ordered phases. In Sec. IV, we find that the isotropic model on the triangular lattice, does not possess a critical phase for any interaction strength but could display an ordered phase for sufficiently large interactions. Finally, Sec. V contains a discussion of the various results and conclusions.

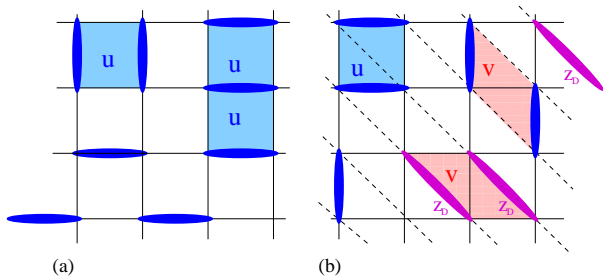


FIG. 1: (Color online) Dimer models a) on the square lattice, with dimer interactions  $u$  on square plaquettes; b) on an anisotropic triangular lattice, with dimer interactions  $u$  and  $v$  on square and diamond-like plaquettes respectively and a fugacity  $z_D$  for dimers on diagonal links.

## II. CRITICALITY OF THE DIMER MODEL ON THE BIPARTITE SQUARE LATTICE

Let us start by reviewing the main results of the square lattice dimer model. In this paper, we will only consider fully-packed dimers with a hard-core constraint: there must be one and only one dimer coming out of each site. The non-interacting model can be solved exactly on the square lattice by expressing the partition function of the system as a Pfaffian, which enables to obtain analytic expressions for the free energy and correlators, on either finite or infinite systems [9, 14]. On the square lattice, dimers are found to be in a critical phase: dimer-dimer correlations decay algebraically as  $1/r^2$  with relative distance  $r$ , whereas the monomer-monomer (defining a monomer as a site with no dimer) correlations behave as  $1/\sqrt{r}$ . Classical dimers on the square lattice have also been studied within a finite-temperature model with nearest neighbors interactions, *i.e.* an interaction  $-u$  between parallel dimers on the same plaquette ( $u > 0$  corresponding to attractive interactions) [12]. Here the model is not integrable anymore and it was found numerically that the system is critical down to a finite temperature  $u_{col}/T = 1.54(3)$ , where it gives rise to a low-temperature columnar phase with dimers aligned in columns. Monomer-monomer correlations decay to 0 at long distances, either algebraically (in the critical phase) or exponentially (in the columnar phase). From now on, unless it is specified otherwise, we set  $T = 1$  and let the different dimer-dimer interactions ( $u$  for the purely square lattice) vary. Nevertheless, we still refer to *high-T* (respectively *low-T*) regions characterized by small (resp.

large) values of the involved couplings.

The criticality encountered in the high-T phase can be understood in the framework of a height field theory. For each dimer configuration on the square lattice, a scalar height field with quantized values (multiples of  $\frac{1}{4}$ ) can be defined microscopically on the dual lattice [15]. The spatial variations of the height field between neighboring sites of the dual lattice are entirely determined by the presence of dimers between them, thanks to the lattice bipartiteness. The long-wavelength modes of this height correspond to a coarse-grained height field  $\Phi(\mathbf{r})$  defined in continuum space, and the physics of the model is captured by the action [12, 16]:

$$S[\Phi] = \int d^2\mathbf{r} g \pi |\nabla\Phi(\mathbf{r})|^2 + V \cos(2\pi p\Phi(\mathbf{r})) \quad (2.1)$$

The cosine term of this action is a *locking potential* that favors  $p$  flat configurations ( $p = 4$  for the square lattice), corresponding microscopically to the columnar configurations. The  $|\nabla\Phi|^2$  term, corresponding to the cost of fluctuations around these flat configurations, account for the entropy of dimer coverings. In the non-interacting case, the value of the stiffness is fixed by the exact results of Ref. [9, 14] to be  $g = \frac{1}{2}$  (see also Ref. [17]). The renormalization of the stiffness constant accounts for the role of interaction:  $g$  increases with  $u$ .

As long as the cosine operator in Eq. (2.1) is irrelevant in the renormalization group sense, this action defines a conformal field theory with central charge  $c = 1$  and the system is critical. The dimer operator (which gives the local dimer density) is composed of a  $\cos(2\pi\Phi)$  and gradient terms [18], and has a scaling dimension  $d_{1,0} = \frac{1}{2g}$ , corresponding to half of the exponent of dimer-dimer correlations. Similarly, the locking potential has a dimension  $d_{p,0} = \frac{p^2}{2g} = \frac{8}{g}$ , and becomes relevant when  $g \geq 4$ . Within the standard Coulomb gas description [19] of this theory, we can define operators corresponding to the insertion of a particle of electric and magnetic charges  $e$  and  $m$  respectively. In general, the dimension of such an electromagnetic vertex operator is  $d_{e,m} = \frac{e^2}{2g} + \frac{gm^2}{2}$ . In the height model discussed here, the operator with  $(e, m) = (1, 0)$  is the dimer operator already mentioned; similarly, the monomer operator corresponds to inserting a magnetic particle with  $(e, m) = (0, \pm 1)$  (the sign of the charge depends on the sublattice where the monomer is inserted). In the critical phase, dimer-dimer and monomer-monomer correlators decay as power laws of the distance and the decay exponents are  $2d_{1,0}$  and  $2d_{0,1}$  respectively. Going back to the height picture, the insertion of magnetic charges (for instance monomers or links breaking the bipartiteness) corresponds to dislocations and, as we show below, can be treated as perturbations in the coarse-grained field theory.

Prior to the presentation of our strategy to attack the

dimer problem, we first introduce the numerical techniques used here and illustrate them on the example of the square lattice interacting dimer model. In this study we use a Transfer Matrix (TM) approach to determine the domains of existence of the different phases of the dimer model, computed on a torus of longitudinal and transverse sizes  $L_\tau$  and  $L$  respectively. The TM techniques allow to compute exponents of critical dimer-dimer and monomer-monomer correlations and also correlations themselves (see Appendix), on systems with  $L_\tau$  large enough to be considered infinite.

For a critical phase such as the one encountered in the high-T region of the square lattice dimer model, we can compute the decay exponents of correlation functions in two ways: either by a direct inspection of the real-space decay of correlation functions (see the description in Sec. 3 of Appendix), or by the leading eigenvalues of the TM (see Sec. 4 of Appendix). Both methods are guided by a conformal field theory (CFT) analysis of the critical phase, and the latter is more precise to determine exponents as it allows to use efficiently topological and translation symmetries of the TM (see Sec. 4 in Appendix). The calculations of correlation functions in real space offer however the advantage of providing more physical informations (for example about the correlation length) when the system is not critical. Another important quantity, namely the central charge  $c$  of the CFT, can also be extracted from the finite-size scaling of the TM largest eigenvalue when the system is critical (see Sec. 4 of Appendix).

We illustrate the validity of this numerical approach in Fig. 2, where the critical phase is evidenced by the  $c = 1$  plateau of the central charge (estimated using TM largest eigenvalues for system widths up to  $L = 14$ ). The scaling dimensions of dimer  $d_{1,0}$  and monomer  $d_{0,1}$  operators (obtained from subleading eigenvalues) are also displayed according to the discussion above, the transition to the columnar phase is characterized by a value  $g = 4$  of the stiffness, thus a value  $d_{1,0} = 1/8$ . This criterion is used to estimate the transition temperature (estimates of  $d_{0,1}$  can also be used in principle, but they are more sensitive to finite-size effects in that temperature range). The results of Fig. 2 lead to an estimate  $u_{\text{col}} = 1.563(7)$ , in good agreement with previous results [12, 13].

### III. CRITICAL PHASE IN A DIMER MODEL INTERPOLATING THE SQUARE AND TRIANGULAR LATTICES

In this section, we investigate whether the bipartiteness of the square lattice is a condition for the existence of the critical phase, by building a model defined on a lattice interpolating continuously between the square and the triangular lattices.

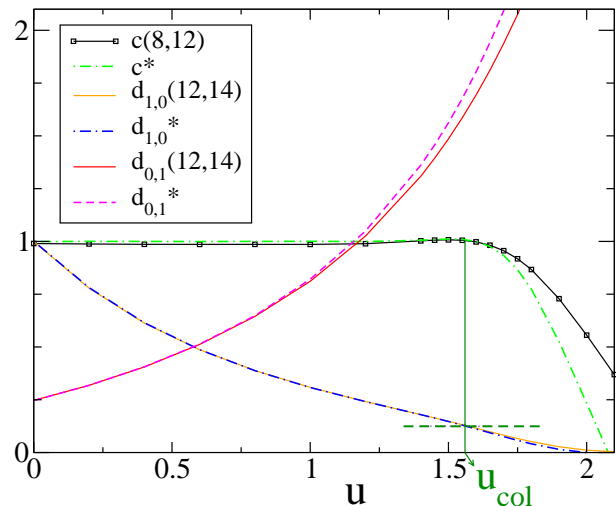


FIG. 2: (Color online) Estimates and extrapolations from different estimates (see Appendix for details and notations) of the central charge  $c$  and of the scaling dimensions  $d_{1,0}$  and  $d_{0,1}$  in the dimer model on the square lattice as a function of interaction strength  $u$ .

*Definition of a model with lattice and interaction anisotropies* — For commodity, we represent the triangular lattice as a deformed square lattice with bonds in the  $x$ ,  $\tau$  and  $\tau - x$  direction (see Fig. 1 and Appendix). The interpolation between both lattices is made by assigning a fugacity  $z_D$  to the diagonal bonds. Since the elementary plaquettes of the triangular lattice are more numerous than those of the square, we need to define another parameter  $v$  characterizing the interaction on *diamond-like* plaquettes (*i.e.* non-square four-site plaquettes). We finally keep the notation  $u$  for the interaction between parallel dimers on a square plaquette. These elementary energy scales in the problem are illustrated in Fig. 1. For  $z_D = 0$  and  $v = 0$ , we have the classical dimer model on the square lattice discussed in Sec. II, while the pure triangular dimer model (that will be discussed in Sec. IV) corresponds to both  $z_D = 1$  and  $v/u = 1$ . To describe the system in function of these two anisotropy parameters, we take the approach of varying either  $z_D$  or  $v/u$  while keeping the other parameter constant. The different paths in the  $(z_D, v/u)$  space where phase diagrams were computed numerically are represented in Fig. 3.

*Description of expected phases and transitions* — In the non-interacting limit ( $u = v = 0$ ) of the present model, the system is disordered with exponentially decaying correlations for any fugacity  $z_D > 0$ : criticality is destroyed by an infinitesimal proportion of diagonal bonds [11]. This can be accounted for in the height field theory by adding a relevant term in the action Eq. (2.1), which can be understood by noticing that adding a single diagonal dimer on the square lattice corresponds to inserting two monomers on the same sublattice, *i.e.* two

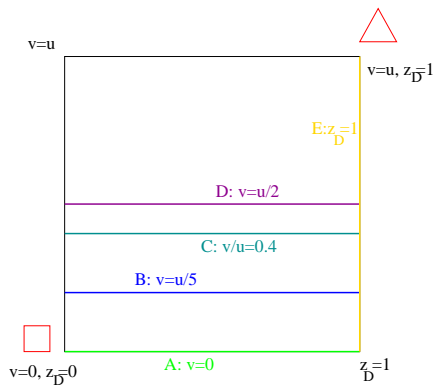


FIG. 3: (Color online) Different parameter-space paths (A to E) taken in the TM calculations in section III.

magnetic charges of the same sign [20]. The corresponding  $m = 2$  vertex operator is written in terms of the field  $\Theta$ , dual to the height field  $\Phi$ , and leads to the new effective action:

$$S[\Phi] = \int d^2\mathbf{r} \pi g |\nabla\Phi(\mathbf{r})|^2 + V \cos(8\pi\Phi(\mathbf{r})) - \lambda \cos(2\Theta(\mathbf{r})) \quad (3.1)$$

In the absence of interactions, this new perturbing field (the  $\cos(2\Theta)$  term) corresponds to the mass term of the free Majorana doublet arising in the large scale regime within the Pfaffian description of the dimer model [11]. For a generic value of the stiffness, the scaling dimensions of the two perturbing terms are  $d_{4,0} = \frac{8}{g}$  and  $d_{0,2} = 2g$  respectively. The fact that the introduction of diagonal bonds is indeed relevant in the non-interacting limit is seen from the value of the stiffness in this case  $g = \frac{1}{2}$  (since  $d_{0,2} = 1 < 2$ ). However, the key point of our study is that the  $\cos(2\Theta)$  term becomes irrelevant for  $g > 1$  whereas the locking potential is relevant only for  $g \geq 4$ . As we can tune the stiffness constant by modifying the interaction strength between parallel dimers ( $u$  and  $v$  terms), we are hoping to reach the  $1 < g < 4$  window, *i.e.* a critical phase on the triangular lattice, within the interacting dimer model defined above. The predicted phase diagram is therefore as follows: first, a high- $T$  liquid phase (for  $1/2 < g < 1$  in the unperturbed model), then a transition to a critical phase ( $1 < g < 4$ ) at intermediate couplings and finally a low- $T$  columnar ordered phase (for  $g > 4$ ). The dimer  $d_{1,0}$  and monomer  $d_{0,1}$  scaling exponents are predicted to be both equal to  $1/2$  at the transition from the liquid to the critical phase, and  $1/8$  and  $2$  respectively at the critical-columnar transition. In both cases, transitions out of the critical phase are expected to be of Kosterlitz-Thouless type. This analysis holds only in the perturbative regime for the diagonal dimer fugacity  $z_D \ll 1$ , and we now address the question whether this scenario is realized for an arbitrary lattice anisotropy  $0 < z_D \leq 1$  by means of numerical TM calculations.

*Perturbation of the square lattice model by diagonal bonds* — We first consider the model with no additional interactions  $v = 0$  and turn on the diagonal dimer fugacity (path A in Fig. 3). Our numerical estimates of the central charge  $c$  and exponents  $d_{1,0}$  and  $d_{0,1}$  are displayed in Fig. 4 as a function of the coupling strength  $u$  for the specific value  $z_D = 0.4$ . We clearly observe the emergence of a  $c = 1$  plateau witnessing a critical phase, for a wide range of couplings. The points  $u_1$  and  $u_2$  where  $d_{1,0} = 1/2$  and  $d_{0,1} = 1/2$  correspond roughly to the high- $T$  limit of the  $c = 1$  plateau, as predicted above; from these criteria, the transition between the critical and liquid phase is located at  $u^* = (u_1 + u_2)/2 = 0.80(5)$ , the error bar being estimated by  $(u_2 - u_1)/2$ . Similarly, the low- $T$  end of the plateau at  $u_{col} = 1.566(8)$ , corresponding to the entrance into the columnar phase, coincides with the criterion  $d_{1,0} = 1/8$ , confirming the analysis above. We use estimates of  $d_{1,0}$  to locate the columnar transition, since as on the square lattice estimates of the monomer exponent  $d_{0,1}$  are more affected by finite-size effects.

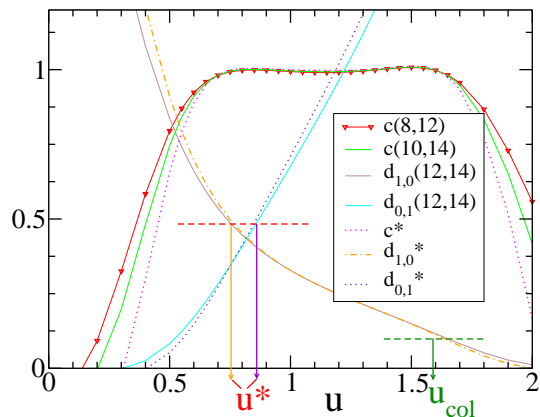


FIG. 4: (Color online) Central charge  $c$ , estimates and extrapolations of the dimer exponent  $d_{1,0}$  and monomer exponent  $d_{0,1}$ , as a function of  $u$  for a diagonal dimer fugacity  $z_D = 0.4$  and  $v = 0$ .

Repeating the same analysis for different values of the diagonal dimer fugacity, we obtain, as a function of  $z_D$  and  $u$ , the phase diagram of Fig. 5. The main features are: (i) the transition temperature to the columnar phase is essentially not affected by the diagonal dimer fugacity and remains close to the value obtained in the square lattice; (ii) as found in Ref. 11, the system with no interaction  $u = 0$  is a gapped liquid irrespective of the diagonal dimer fugacity; (iii) the dimer model (with  $v = 0$ ) comprises a critical phase even on the isotropic triangular lattice ( $z_D = 1$ ), where it extends from  $u^* = 1.08(5)$  up to  $u_{col} = 1.575(10)$ .

These results are in full agreement with the predictions of the field-theoretical analysis developed above. We emphasize also here that the lattice bipartiteness is not a necessary condition to have criticality in a dimer model,

and that this condition should rather be replaced by a condition on the existence of a stiffness constant window  $1 < g < 4$  in an unperturbed model.

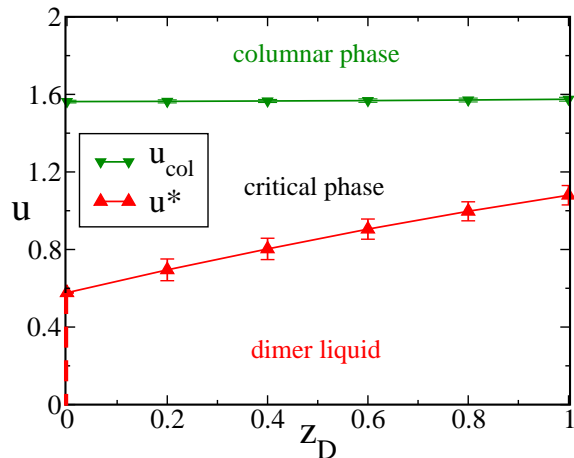


FIG. 5: (Color online) Phase diagram for  $v = 0$  (line A in Fig. 3) as a function of diagonal dimer fugacity  $z_D$  and square-plaquettes interaction  $u$ . Note that on the  $z_D = 0$  line, the small  $u$  region also corresponds to a critical phase (dashed line).

*Introduction of a finite interaction anisotropy  $v/u$*  — We now introduce the interaction term  $v$  on the diamond-like plaquettes. The  $u$  and  $v$  terms are in competition, since they tend to favor different dimer orderings. When  $v < u$ , the square columnar configurations will eventually dominate at low enough  $T$ , but the presence of the frustrating  $v$  interactions will shift down the transition temperature to the ordered phase. As the algebraic correlations of the critical phase also correspond to a square-like columnar ordering at lower temperatures, we also expect the extent of the critical phase to shrink down as the strength of the  $v$  interactions is increased. From the point of view of the effective action Eq. (3.1), we expect  $g$  to *decrease* with the  $v$  frustrating interactions.

For a sufficiently small  $v/u$  parameter, the behavior of the system is found to be identical to the case  $v = 0$ , with a critical phase, evidenced by a  $c = 1$  plateau between the dimer liquid and the ordered phase. This is illustrated in Fig. 6 for anisotropy parameters  $(z_D, v/u) = (0.4, 0.2)$ . As expected, the transition towards the ordered phase is slightly shifted towards lower temperatures ( $u_{\text{col}} = 1.624(8)$  for  $v/u = 0.2$  while  $u_{\text{col}} = 1.566(8)$  for  $v = 0$ ). The high-T boundary of the critical phase is more strongly affected by the presence of  $v$  interactions: for the same lattice anisotropy,  $u^* = 0.92(6)$  for  $v/u = 0.2$  to be compared with  $0.80(5)$  for  $v = 0$ .

Using the same procedure as before, the transition points  $u^*$  and  $u_{\text{col}}$  were determined in the regions of the phase diagram corresponding to paths B,C,D (with respectively  $v/u = 0.2, 0.4$  and  $0.5$ ), and E (for  $z_D = 1$ ) and

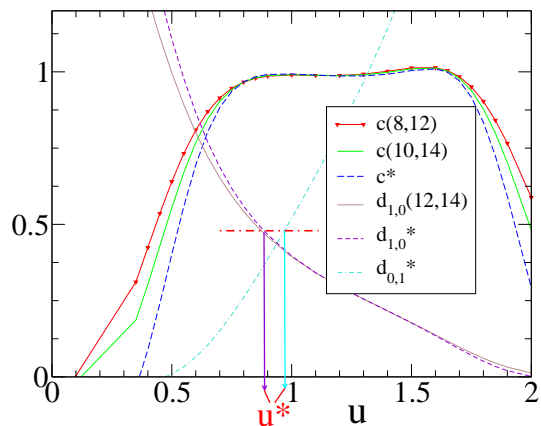


FIG. 6: (Color online) Central charge and exponents (estimates and extrapolations) for an interaction anisotropy  $v/u = 0.2$  and diagonal dimer fugacity  $z_D = 0.4$ .

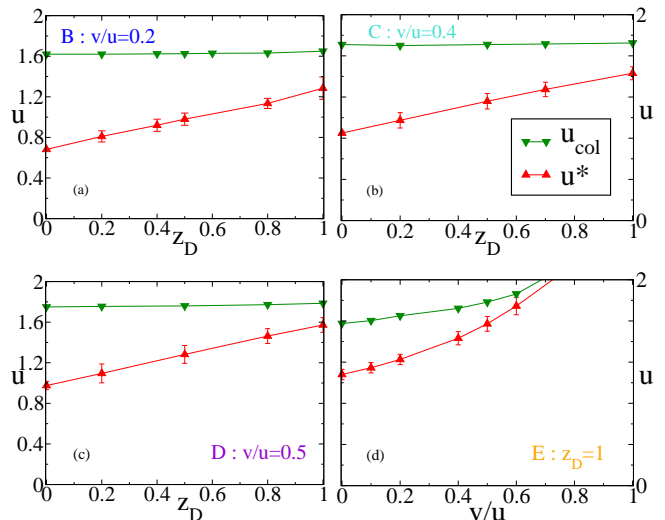


FIG. 7: (Color online) Phase boundaries  $u^*$  and  $u_{\text{col}}$  as a function of either  $z_D$  [(a), (b) and (c)] or  $v/u$  [(d)], corresponding respectively to the paths B, C, D and E in Fig. 3. Error bars on  $u_{\text{col}}$  are smaller than symbol size.

the corresponding phase diagrams are reported in Fig. 7. As anticipated, we clearly see that the effect of adding the interaction  $v$  is essentially to shift both boundaries of the critical phase towards lower temperatures: in other words, the frustration due to the  $v$  terms has a net tendency to stabilize the dimer liquid and to destabilize the ordered (columnar) or quasi-ordered (critical) phase. For a given fugacity  $z_D$ , the extent of the critical phase indeed decreases as  $v/u$  increases. The transition between the dimer liquid and the critical phase turns out to be more affected by  $v/u$  than the transition towards the columnar phase. We can interpret this with the following rough argument:  $v$  interactions effectively increase the weight of diagonal bonds in the dominant configurations, enhanc-

ing the perturbation caused by the diagonal bonds and therefore decreasing the extent of the critical phase from the high- $T$  direction.

For large values of  $v/u$ , a fair determination of phase boundaries becomes more difficult as finite-size effects are getting more important. For instance, the determination of  $u^*$  with the dimer and monomer exponents criteria give values increasingly far from each other, resulting in larger error bars in the phase diagrams of Fig. 7c and d. In practice for  $v/u > 0.5$ , both our numerical results and the way of analyzing them break down due to uncontrolled finite size effects. This is actually not a surprise, as the CFT-guided analysis of the TM results (see Sec. 4 in Appendix) relies on the existence of an unperturbed critical window in the model, which is no longer present for large  $v$  interactions. For  $v/u > 0.5$ , we also find that the second largest TM eigenvalue is no more found in the  $q = \pi$  symmetry sector in the low- $T$  phase. This indicates a change in nature of the lowest-energy excitations and that the scheme along which criticality was previously understood is not valid anymore. From these arguments and even if our finite-size results become less reliable, it is clear that they are no longer compatible with the existence of an extended critical phase for  $v/u > 0.5$ : this is exemplified by the absence of a plateau in the numerical estimate of the central charge. Finally, we note that in parallel to the shrinking of the critical phase observed when increasing  $v/u$ , the columnar transition seems to be progressively shifted towards the  $T = 0$  limit as the interaction anisotropy parameter approaches 1 (see Fig. 7d). This is again in agreement with our previous qualitative arguments on the effect of  $v$  interactions.

#### IV. DIMER ORDERING ON THE ISOTROPIC TRIANGULAR LATTICE

We now turn to the more complex situation of the isotropic triangular model, where  $z_D = 1$  and  $v = u$  (in this section, the isotropic interaction will only be denoted by  $u$ ). The high- $T$  limit is in this case well understood: the system is in a dimer liquid phase, with exponentially decaying dimer-dimer and monomer-monomer correlation functions. This has been shown exactly for  $u = v = 0$  in Ref. 11, and we could confirm it for small values of the interaction strength. For intermediate  $u = v$  values, as expected from the results of Sec. III for  $v/u > 0.5$ , we find no evidence for a critical phase in our TM calculations (in particular, no  $c = 1$  plateau).

Whereas we always found a low- $T$  columnar ordering up to now, the low- $T$  behavior of the isotropic triangular model reveals more complex. Indeed, from the isotropy of the interactions and since all dimer fugacities are equal, it appears that configurations that minimize the energy are more numerous. At first glance,

12(=  $6 \times 2$ ) columnar ordered ground-state configurations emerge (6 for the number of ways to put a dimer on a link connected to a given site and 2 for the possible directions of a dimer column, given an orientation of dimers). However, as first remarked in Ref. 10, the number of configurations that minimize the energy is much larger as one can easily create zero-energy defects by just translating a line of dimers or flipping all dimers along a column. These two types of moves from a given columnar ground-state are represented in Fig. 8. The almost extensive ground-state degeneracy generated by these costless defects clearly changes the picture for the low- $T$  behavior of the isotropic triangular dimer model. Indeed, at  $T = 0$ , strictly speaking, the system is no longer ordered with respect to a local order parameter such as the columnar one defined for the square lattice. However, it is still possible that at finite  $T$ , the thermal fluctuations select a specific ordering pattern: this would be an illustration of the “order by disorder” effect [21, 22].

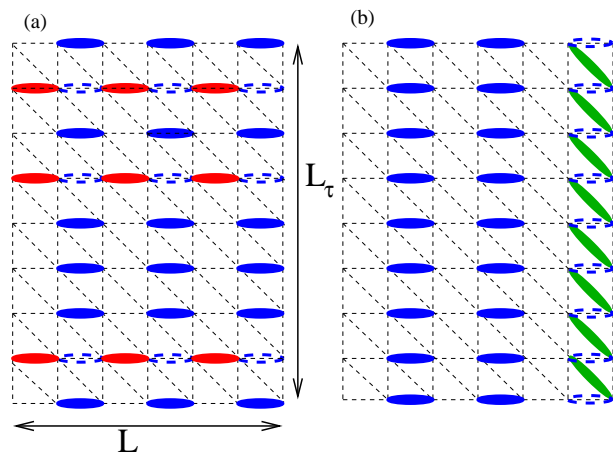


FIG. 8: (Color online) Different types of zero-energy defects on the (isotropic) triangular lattice dimer model, from a specific columnar ordered ground-state: (a) *line-shifting modes*; (b) *column-flipping modes*.

In fact, for the quantum dimer model on the triangular lattice, Moessner and Sondhi found in perturbation theory (with respect to the quantum kinetic terms) that indeed (quantum) fluctuations select the 12 ordered columnar states [10]. Noticing that in our classical model, *thermal* fluctuations play the same role as *quantum kinetic* fluctuations in the quantum dimer model [12] since both essentially count the number of flippable plaquettes in a given state, it is likely that thermal fluctuations (instead of quantum fluctuations) trigger a similar order-by-disorder scenario here. From general arguments [22], we expect that if it is indeed the case, the transition temperature to the columnar phase should be quite low. It could also happen that, for our specific model, this transition never occurs and the systems stays in a liquid phase down to  $T = 0$ .

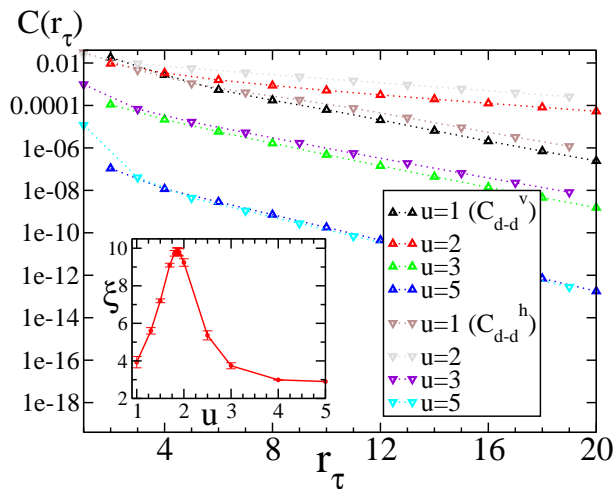


FIG. 9: (Color online) Connected dimer-dimer correlations as a function of the distance  $r_\tau$  along the main axis of a torus of dimensions  $(L_\tau, L) = (60, 6)$ , for interaction strengths  $u$  between 1 and 5. Correlations of vertical (respectively horizontal) dimers are represented by up (resp. down) triangles. For clarity, we only displayed horizontal (resp. vertical) dimer correlations at odd (resp. even) distances. Inset: estimated correlation length  $\xi$  as a function of  $u$ .

We now try to settle this issue with the help of numerical TM calculations. As the critical phase disappeared, we can no longer use the CFT-based analysis of the previous sections and we have to resort to more standard thermodynamical means of detecting the hypothetical transition to a low- $T$  ordered phase. We first computed dimer-dimer correlations by TM iterations (see Appendix). In Fig. 9, connected correlation functions are displayed as a function of dimer-dimer distance  $r_\tau$  for the example of a  $(L_\tau, L) = (60, 6)$  torus for interaction strength  $u$  up to 5. As exemplified by the log-linear scale, they are clearly short-ranged with an exponential decay (plus an oscillating part depending on the parity of  $r_\tau$ ). We obtain an estimate of the correlation length  $\xi$  by fitting the correlations to an exponential decay  $\exp(-r_\tau/\xi)$ . The resulting curve  $\xi(u)$ , displayed in the inset of Fig. 9, shows a well-pronounced peak at a finite value of  $u$ , which could correspond to an ordering temperature. We also find that the peak positioned at  $u = 1.9(1)$  for the system size  $L = 6$ , shifts towards higher interaction strength  $u = 2.22(5)$  for  $L = 8$ .

Another thermodynamical insight is given by the specific heat per site  $c_v = \frac{1}{L \cdot L_\tau} d\langle E \rangle / dT$ , which is also accessible to the TM calculations (see Sec. 2 of Appendix for details). Fig. 10 displays the specific heat as a function of  $u$  for different system widths  $L$ . For each value of  $L$ , the specific heat peaks at a temperature close to the ones of the  $\xi(u)$  curves. As  $L$  increases, the peak in  $c_v(u)$  sharpens and shifts to lower temperatures. We discuss below the finite-size scaling of the position of the

peak but already note at this stage that the clear narrowing of the specific heat peak with increasing system size, conjugated with the absence of a power-law envelop, is very suggestive of a *first-order* phase transition.

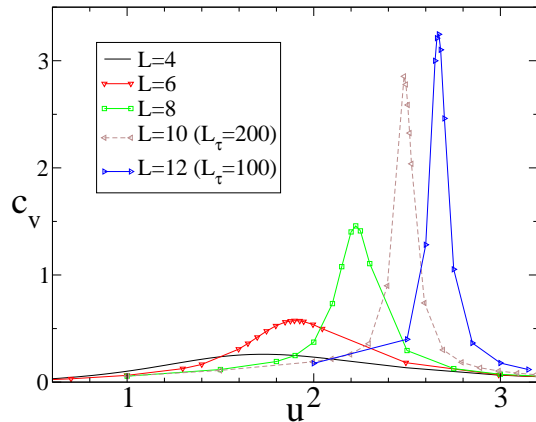


FIG. 10: (Color online) Specific heat per site  $c_v = \frac{1}{L \cdot L_\tau} \frac{d\langle E \rangle}{dT}$  as a function of  $u$  for systems of different widths (see Appendix for details of computation).

Having possible signs of a phase transition, we now try to find an order parameter for the low- $T$  phase. As already discussed, this is not a simple task because of the zero-energy modes that are responsible for the large ground-state degeneracy. The specific geometry of the TM is of help here to characterize the appearance of long-range order. Consider a very long cylinder  $L_\tau \gg L \gg 1$  with PBC in the small  $L$  direction. With this geometry, the ground-states having dimers perpendicular to the long direction (horizontal dimers) are much more numerous than ground-states with only vertical or diagonal dimers. Indeed, there are  $2^{L_\tau}$  horizontal ground-states (corresponding to the *line-shifting modes*, see Fig. 8a). The same line-shifting modes provide only a much smaller ( $2^L$ ) degeneracy for vertical or diagonal ground-states. The other family of low-energy modes (*column-flipping modes*) give a small  $O(2^{L/2})$  degeneracy for the horizontal ground-states (see Fig. 8b), and a  $O(2^{L_\tau/2})$  degeneracy for both vertical and diagonal ground-states. Consequently, in the limit of large  $L_\tau$ , we expect horizontal line-shifting modes to predominate.

If there is long-range order in the system, the previous analysis indicates that the long cylinder geometry induces a preferential ordering in the horizontal dimers (for entropic reasons). Consequently, we consider the average occupation of horizontal bonds on a given line of the lattice as a good indicator of a possible phase transition. At infinite temperature, occupations of all bonds are all likely and equal to  $1/6$ . In contrast, from the arguments above, at very low  $T$ , the probability for a horizontal bond to be occupied on an infinitely long cylinder

is  $P_- = 1/2$ . Defining

$$\langle m \rangle = \frac{P_- - 1/6}{1/2 - 1/6} = 3P_- - \frac{1}{2},$$

we expect the “order parameter”  $\langle m \rangle$  to vanish in the low-coupling limit  $u = 0$  and to saturate to 1 at large enough coupling. Even if, strictly speaking, this above argument is not rigorous (because  $L_\tau$  and  $L$  are both finite in our computations), we expect  $\langle m \rangle$  to reflect a true physical behavior.  $\langle m \rangle$  is shown in Fig. 11 for lattice widths  $L = 4, 6, 8$  and we clearly observe the predicted behavior (saturation to 0 at small  $u$  and to 1 at large couplings). As for the specific heat data, we observe that the shape of  $\langle m \rangle$  is strongly influenced by the system size, with similar trends: as  $L$  increases, the temperature region of ordering (where  $d\langle m \rangle/du$  is maximal) is getting narrower and is shifted towards lower temperatures.

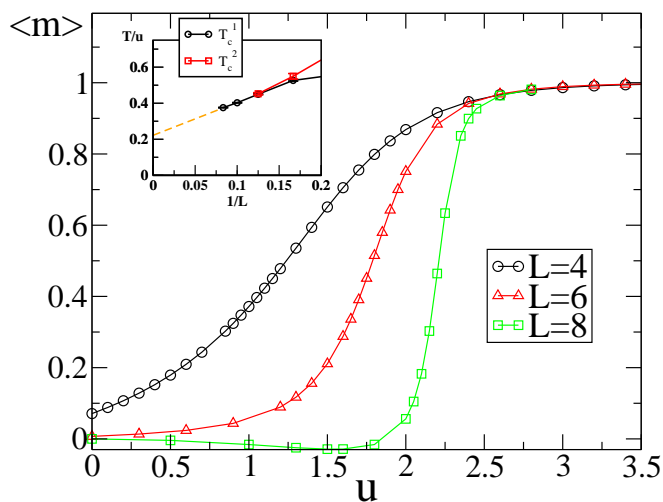


FIG. 11: (Color online) Proposed order parameter  $\langle m \rangle$  for the long cylinder geometry (see text) versus coupling strength  $u$  for different lattice sizes. Inset: finite-size transition temperatures  $T_c^1$  and  $T_c^2$  (maxima of  $c_v$  and  $d\langle m \rangle/du$  respectively) versus  $1/L$ .

In order to have a better understanding of this ordering phenomenon, we have computed the order parameter  $\langle m \rangle$  away from the purely isotropic case, for a diagonal dimer fugacity  $z_D = 1$  but for values of  $v/u$  lower than 1. The evolution of  $\langle m \rangle$  with  $u$  is shown on Fig.12 for different interaction anisotropies  $v/u = 0.4; 0.6; 0.8; 1$ . As soon as  $u$  is larger than  $v$ , the mean occupation of horizontal links  $P_-$  is  $1/4$  at zero temperature, which is consistent with the fact that, as in the purely square columnar state, only 4 configurations have the minimal energy. Nevertheless, the ordering occurring when  $u$  increases is characterized by larger values of  $\langle m \rangle$  in an intermediate temperature range. As  $v/u$  increases, the maximal value of  $P_-$  gets closer to  $1/2$ , which is the value found in the ordered phase discussed previously in the isotropic case. Notice that the extent of the temperature range where  $P_-$  approaches  $1/2$  increases with the length  $L_\tau$  of the system

(see  $v/u = 0.6$  curves in the Fig. 12), which supports the scenario of order by disorder: the  $P_- = 1/2$  asymptotic value can be understood by the number  $O(2^{L_\tau})$  of lowest-energy defects (which are lowest-energy configurations in the isotropic case). With interaction anisotropy, these defects are allowed only at finite temperatures, and proliferate down to lower temperatures as  $u - v$  decreases. This clearly shows that the ordered phase in the isotropic triangular lattice model differs both qualitatively and quantitatively (by the number of lowest-energy configurations) from that of its anisotropic version, and is a good example of the “order by disorder” scenario.

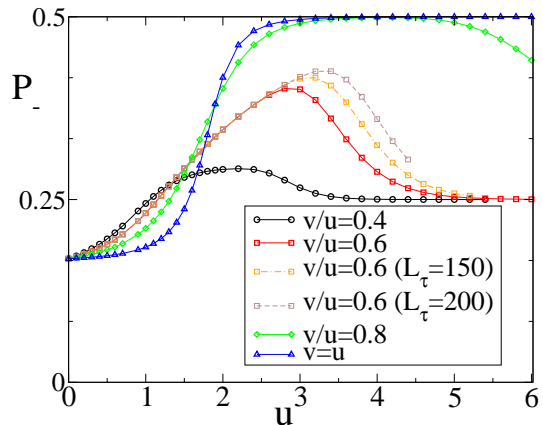


FIG. 12: (Color online) Average occupation  $P_-$  of horizontal bonds computed on a row of an isotropic triangular lattice of dimensions  $L = 6$  and  $L_\tau = 100$  (if not specified), for different interaction anisotropy parameters  $\frac{v}{u} = 0.4; 0.6; 0.8; 1$ , as a function of interaction strength.

At this stage, we have three indications (from the correlation length, the specific heat and  $\langle m \rangle$ ) that the isotropic triangular interacting dimer model could order at low temperatures. In all cases, the transition temperature was seen to decrease quite consequently with system size. To check whether the system could order at finite  $T$  in the thermodynamic limit, we perform a finite-size scaling of these effective transition temperatures. In the insert of Fig. 11, the finite-size temperature transitions  $T_c^1(L)$  and  $T_c^2(L)$  corresponding to respectively the maxima of the specific heat and of  $d\langle m \rangle/du$ , are plotted as a function of inverse transverse system size  $1/L$ . A precise finite-size scaling form is difficult to determine (due noticeably to large error bars), but all reasonable finite size dependence (*e.g.* linear or quadratic in  $1/L$ ) lead to a finite value of  $T_c$  in the thermodynamic limit. A rough estimate can be made with the help of linear interpolation (dashed line on the figure) and gives  $T_c = 0.2 \pm 0.05$  (in units of  $u$ ).

Our numerical results therefore seem to be consistent with a finite temperature ordering of the isotropic lattice model, probably triggered by an order by disorder mechanism [21, 22]. The sharp behavior of both spe-

cific heat and “order parameter” at the transition (see Fig. 11), as well as the absence of any criticality behavior in the central charge, suggests that this transition is first order. We finish by noting that the samples used in the computations are of relatively moderate size, and that it is still possible that the extrapolated transition temperature actually vanishes with larger samples available. To have a better understanding of this transition with the presently available system sizes, one could also study this model on samples with other geometries and adapted order parameters, and check if extrapolations of finite-size temperatures on different geometries give the same  $T_c$  in the thermodynamic limit. Another insight could be given by Monte Carlo simulations for this model. We expect however these simulations to be difficult as the presence of the low-energy modes (and the corresponding large degeneracy of the ground-state) will certainly induce ergodicity and freezing problems in the Monte Carlo process [23]. Such investigations are beyond the scope of the present paper.

## V. CONCLUSIONS

To summarize, we have constructed a simple classical interacting dimer model on a lattice that interpolates between square and triangular lattices. This is of particular interest since the two limiting models singularly exhibit very different behaviors at infinite temperature (critical and short-ranged phases for the square and triangular lattices respectively). Since the topology of the triangular lattice can be simply obtained from the square lattice by adding one extra diagonal bond on each square plaquette, we have introduced a fugacity parameter for these extra bonds. Similarly, the extra bonds leading to new local interactions in diamond-like plaquettes, we have also considered dimer interactions on these plaquettes, differing from those on the square plaquettes.

This anisotropic dimer model has been investigated in great details using simple considerations as well as numerical transfer matrix techniques (on strips with up to 14 sites wide) supplemented by predictions from conformal field theory. A very rich phase diagram has been obtained with, in particular, a novel intermediate behavior where the critical phase is now restricted to a finite intermediate temperature range and does not extend, as for the pure square lattice model, up to infinite temperature. At high-temperature, the critical phase is hence replaced by a liquid dimer phase as in the isotropic triangular lattice. It is of interest that such a behavior appears immediately for arbitrary small fugacity of diagonal bonds so that one can view the typical behavior of the square lattice as a “singular” limit. However, we note that the critical phase itself survives in an extended vicinity of the square lattice model (although its exten-

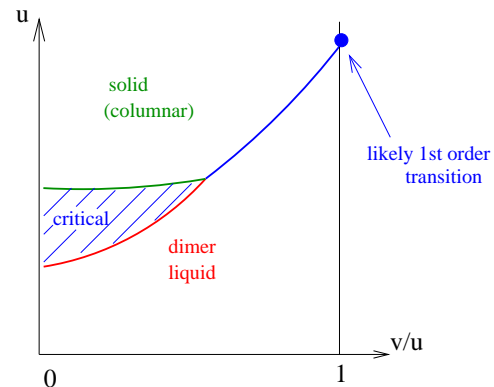


FIG. 13: Schematic projective phase diagram of the dimer model on the triangular lattice ( $z_D = 1$ , line E of Fig. 3), in terms of the interaction  $u$  and interaction anisotropy  $v/u$ .

sion in temperature jumps abruptly) and this stability is therefore *not* related to the bipartiteness of the lattice. While the critical phase disappears progressively with increasing interaction anisotropy, the ordered phase survives for any range of anisotropy, as well as the high-T liquid dimer. Criticality in this model hence requires to have sufficiently anisotropic interactions. These findings are reproduced in the schematic phase diagram of Fig. 13 for the case of isotropic dimer fugacity  $z_D = 1$ . Lastly, we have devoted special attention to the limiting case of the isotropic dimer model on the triangular lattice where we found evidence of a direct (likely first-order) transition between the high-T liquid phase and a low-T ordered phase triggered by an order-by-disorder mechanism.

## Acknowledgments

We thank F. Becca, S. Capponi and C. Castelnovo for fruitful discussions, the *Agence Nationale de la Recherche* (France) for support and IDRIS (Orsay, France) for computer time.

## TRANSFER MATRIX ANALYSIS OF THE ANISOTROPIC DIMER MODEL

Other works [12, 13] already discussed the construction of the TM for an interacting dimer model. We give a few technical details related to the triangular lattice and to the observables studied in the body of the text.

$L$	$\dim(\mathbf{T}^e(q=0))$	$\dim(\mathbf{T}^e(q=\pi))$	$\dim(\mathbf{T}^o(q=0))$
8	424	421	410
10	2980	2929	2954
12	22218	22207	22150
14	170980	170665	170822

TABLE I: Dimensions of the TM restricted by translation invariance to symmetry sectors of wave vectors  $q = 0$  and  $q = \pi$ , and by topological invariance to *even* and *odd* sectors, for system widths  $L$  up to 14.

### 1. 1D and 2D dimer configurations

The TM allows to treat a 2D  $L \times L_\tau$  system with periodicity in the transverse direction ( $x$ ) as a succession of  $L_\tau$  1D rows of lengths  $L$ . In a row at abscissa  $\tau$  (the  $\tau$  axis being the direction of propagation of the TM), a dimer configuration  $C$  is specified by the dimer occupation of horizontal (oriented along  $\mathbf{e}_x$ ) links at abscissa  $\tau$  and of vertical and diagonal links connecting sites at abscissa  $\tau$  to sites at  $\tau+1$ , at relative positions  $\mathbf{e}_\tau$  and  $\mathbf{e}_\tau - \mathbf{e}_x$  respectively. The number of such configurations, which is the size of the TM, is  $3^L$  (This number can be evaluated as  $\text{Tr}(\mathbf{M}^L)$  where  $\mathbf{M}$  is a *one-dimensionnal transfer matrix* defined between the 4 dimer configurations allowed on a triangle, taking into account the hard-core constraint).

The topology of the triangular lattice is such that on a  $L$ -wide cylinder, the parity of the number of vertical or diagonal dimers linking two successive rows is conserved along the  $\tau$  axis (assuming that  $L$  is even). This defines two topological sectors (*even* and *odd*), and the TM is block-diagonal with corresponding blocks  $\mathbf{T}^e$  and  $\mathbf{T}^o$  respectively. We also use the invariance by translation along the  $x$  axis to reduce the size of  $\mathbf{T}$ . Translation invariance allows to consider, instead of  $3^L$  1D configurations, only their representatives in a symmetry sector (defined by the transverse wave vector  $q$ ), from which other configurations are obtained by translations along  $\mathbf{e}_x$ . Note that the TM elements take into account not only representatives but also all configurations connected to a given representative. These two invariances allow to reduce considerably the TM size in various symmetry and topological sectors. We give in Table I the size of the different sectors useful in the following for  $L$  up to 14. Values of non-zero TM elements, *i.e.* between compatible 1D-configurations, depend on the number of doubly occupied plaquettes of both types and of diagonal links occupied in these configurations.

### 2. Partition function and correlation functions

With the transfer matrix  $\mathbf{T}$  constructed, we have access to statistical properties of the model on a  $L \times L_\tau$

torus by means of the partition function, which reads

$$Z(u, v, z_D) = \text{Tr}(\mathbf{T}^{L_\tau}) = \sum_{C_1, C_2, \dots, C_{L_\tau}} \mathbf{T}_{C_1, C_2} \dots \mathbf{T}_{C_{L_\tau}, C_1}$$

*Internal energy and specific heat* — From the TM elements, one also gets the internal energy of the system:

$$\langle E \rangle = -\frac{1}{Z} \sum_{C_1, C_2, \dots, C_{L_\tau}} \mathbf{T}_{C_1, C_2} \dots \mathbf{T}_{C_{L_\tau}, C_1} \ln(\mathbf{T}_{C_1, C_2} \dots \mathbf{T}_{C_{L_\tau}, C_1}).$$

We computed the specific heat per site  $c_v = \frac{1}{L \cdot L_\tau} d\langle E \rangle / dT$  by a numerical differentiation of  $\langle E \rangle$  with respect to the inverse of the coupling strength. For the calculations of Sec. IV,  $\langle E \rangle$  was computed exactly for  $L = 4, 6, 8$ -wide systems (with  $L_\tau \gg L$  so that  $c_v$  does not depend on  $L_\tau$ ). For wider systems  $L = 10, 12$ ,  $\langle E \rangle$  was estimated by searching the leading TM eigenvector and evaluating from it the energy per row  $\langle E \rangle / L_\tau$  (the consistency of this method, valid in the limit of infinitely long systems, was checked for  $L = 8$  first).

*Correlation functions* — Correlation functions are computed by means of TM iterations. Dimer-dimer correlations, for two dimers with a specified orientation and relative position  $\mathbf{r}$ , are obtained as the ratio over the partition function  $Z$  of a modified partition function  $Z'$  taking into account only the 2D-configurations where these two dimers are present. Mathematically, a projector  $\mathbf{P}$  onto the corresponding 1D configurations is inserted in the matrix product in  $Z'$  at positions corresponding to both dimers:

$$C(\mathbf{r}) = \frac{Z'}{Z} = \frac{\text{Tr}(\mathbf{P} \mathbf{T}^{r_\tau} \mathbf{P} \mathbf{T}^{L_\tau - r_\tau})}{\text{Tr}(\mathbf{T}^{L_\tau})}$$

where  $r_\tau$  is the projection onto the  $\tau$  axis of the relative position  $\mathbf{r}$ . Even if we do not discuss them in the body of the text, monomer-monomer correlations are also accessible via TM calculations. In the TM language, the insertion of a monomer in a given row requires to replace the TM by a modified matrix  $\mathbf{T}'$  which forbids the occupation of links emerging from this site (this involves a change of topological sector). For both dimer-dimer and monomer-monomer correlations, we checked that in the non-interacting case, the exact results of Ref. 11 are recovered.

### 3. Analysis of real-space correlations

When the system is in a critical phase, conformal transformation techniques [24] can be used to analyze the real-space decay of correlation functions on a  $L$ -wide infinite cylinder. Consider the correlation of two dimers

(or monomers) located at a relative distance  $r_\tau$  along the cylinder axis. If the exponent of the infinite-plane power-law correlations is  $2\alpha$ , correlations on the cylinder scale as:

$$C(r_\tau) \sim \left( \cosh\left(\frac{2\pi r_\tau}{L}\right) - 1 \right)^{-\alpha},$$

which can be approximated, for distances much larger than  $L/(2\pi)$ , by an exponential decay with a correlation length  $L/(2\pi\alpha)$ . We checked our calculations on the non-interacting case on the square lattice for a  $L = 6$  cylinder. We found a correlation length  $\xi = 1.02(2)$ , close to the expected (thermodynamical limit) value  $L/(2\pi d_{1,0}) = 3/\pi \sim 0.95$ . The small discrepancy can be attributed to the  $1/r^4$  correction present in the correlation function [14]. Repeating the same calculations for monomer correlations, we extracted from the exponential decay a critical exponent  $d_{0,1} \sim 0.26$ , in good agreement (for such a small  $L$  value) with the exact value  $1/4$ .

#### 4. CFT analysis of largest TM eigenvalues

The CFT analysis is also useful to compute the central charge  $c$ , as well as the scaling dimension of the dimer  $d_{1,0}$  and monomer  $d_{0,1}$  operators, from the size dependence of the leading TM eigenvalues [12]. The central charge is estimated by the  $L$ -dependence of the largest eigenvalue  $\Lambda_0$  of  $\mathbf{T}$ , which is directly connected to the free energy per site  $f_0$ , in the limit of an infinitely long system:

$$f_0 = -\frac{1}{L} \ln(\Lambda_0) = f^* - \frac{\pi c}{6L^2} + o\left(\frac{1}{L^2}\right).$$

In practice, we add a  $\frac{1}{L^4}$  term to the previous fitting expression [13], which is justified by symmetry reasons and improves the agreement between raw data and the fitted expression of  $f_0$ . Estimating  $c$  thus requires to perform

a fit of  $f_0$  with at least 3 values of  $L$ . The size of the TM is a limitation to the number of sizes accessible; nevertheless, one can use the already mentioned topological and translation invariance to address larger sizes. Indeed, one can assert by symmetry reasons and check numerically that the leading eigenvalue of the TM is found in the  $q = 0$  *even* sector. The scaling dimensions of dimer and monomer exponents are determined from the largest eigenvalues in other symmetry sectors [12]:

$$\begin{aligned} -\frac{1}{L} \ln \left( \frac{\Lambda_0^e(q = \pi)}{\Lambda_0^e(q = 0)} \right) &= \frac{2\pi d_{1,0}}{L^2} + O\left(\frac{1}{L^4}\right) \\ -\frac{1}{L} \ln \left( \frac{\Lambda_0^o(q = 0)}{\Lambda_0^o(q = 0)} \right) &= \frac{2\pi d_{0,1}}{L^2} + O\left(\frac{1}{L^4}\right). \end{aligned}$$

This allows to determine  $c$  and  $d_{e,m}$  (with  $(e + m = 1)$ ) from the power method [25], requiring less memory than for a full diagonalization. To minimize finite-size effects on  $c$  and  $d_{e,m}$ , we use different estimates for these quantities. Each estimate is the result of a fit with either 3 (for  $c$ ) or 2 (for  $d_{e,m}$ ) consecutive values of  $L/2$ . In this way one obtains estimates  $c(L - 4, L)$  and  $d_{e,m}(L - 2, L)$  (for  $L \leq 14$ ). The finite-size effects on these estimates become smaller when increasing  $L$ ; in order to obtain more reliable values we make extrapolations of these estimates, assuming that they scale as [13]:

$$\begin{aligned} c(L - 4, L) &\sim c^* + \frac{K}{(L - 4)^2} \\ d_{e,m}(L - 2, L) &\sim d_{e,m}^* + \frac{K'}{(L - 2)^2} \end{aligned}$$

Such estimates and their extrapolations are displayed in Fig. 2, 4 and 6. In general, the  $c^*$  extrapolations were done with estimates  $c(8, 12)$  and  $c(10, 14)$ , while for  $d_{e,m}^*$  extrapolations we used the estimates  $d_{e,m}(8, 10)$ ,  $d_{e,m}(10, 12)$  and  $d_{e,m}(12, 14)$ . The difference between the extrapolation and the closest estimate (the one with the largest  $L$ ) gives the order of magnitude of the error.

- 
- [1] D. S. Rokhsar and S. A. Kivelson, Phys. Rev. Lett. **61**, 2376 (1988).
  - [2] M.E. Fisher, J. Math. Phys. **7**, 1776 (1966).
  - [3] R. Moessner, S.L. Sondhi, Phys. Rev. B **68**, 054405 (2003).
  - [4] F. Vernay, A. Ralko, F. Becca and F. Mila, Phys. Rev. B **74**, 054402 (2006).
  - [5] M. E. Zhitomirsky, Phys. Rev. B **71**, 214413 (2005).
  - [6] D.L. Bergman, R. Shindou, G.A. Fiete, L. Balents, Phys. Rev. Lett. **96**, 097207 (2006); D.L. Bergman, G.A. Fiete, L. Balents, Phys. Rev. B **73**, 134402 (2006).
  - [7] A. Sen, K. Damle and T. Senthil, preprint cond-mat/0701476.
  - [8] D. Poilblanc, K. Penc and N. Shannon, preprint cond-mat/0702367.
  - [9] P.W. Kasteleyn, Physica **27**, 1209 (1961); H.N.V. Temperley and M.E. Fisher, Phil. Mag. **6**, 1061 (1961); M.E. Fisher, Phys. Rev. **124**, 1664 (1961).
  - [10] R. Moessner and S.L. Sondhi, Phys. Rev. Lett. **86**, 1881 (2001).
  - [11] P. Fendley, R. Moessner, S.L. Sondhi, Phys. Rev. B **66**, 214513 (2002).
  - [12] F. Alet *et al.*, Phys. Rev. Lett. **94**, 235702 (2005); Phys. Rev. E **74**, 041124 (2006).
  - [13] C. Castelnovo, C. Chamon, C. Mudry, and P. Pujol, Ann. Phys. **322/4**, 903 (2007); see also D. Poilblanc *et al.*, Phys. Rev. B **74**, 014437 (2006).
  - [14] M. Fisher, J. Stephenson, Phys. Rev. **132**, 1411 (1963).
  - [15] H.W.J. Blöte and H.J. Hilhorst, J. Phys. A **15**, L631 (1982).

- [16] J. Kondev and C.L. Henley, Phys. Rev. B **52**, 6628 (1995); Nucl. Phys. B **464**, 540 (1996); C. Zeng and C.L. Henley, Phys. Rev. B **55**, 14935 (1997); R. Raghavan, C.L. Henley and S. L. Arouh, J. Stat. Phys. **86**, 517 (1997).
- [17] C.L. Henley, J. Stat. Phys. **89**, 483 (1997).
- [18] E. Fradkin *et al.*, Phys. Rev. B **69**, 224415 (2004).
- [19] B. Nienhuis, in *Phase transitions and Critical Phenomena*, edited by C. Domb and J. L. Lebowitz (Academic, London, 1987), Vol. 11.
- [20] C. Castellano, C. Chamon, C. Mudry, and P. Pujol, Phys. Rev. B **73**, 144411 (2006).
- [21] J. Villain, R. Bidaux, J.-P. Carton and R. Conte, J. Phys. **41** 1263, (1980)
- [22] E.F. Shender, P.C.W. Holdsworth in *Fluctuations and order: a new synthesis*, edited by M.M. Millonas (Springer-Verlag, 1996)
- [23] C. Castellano, P. Pujol and C. Chamon, Phys. Rev. B **69**, 104529 (2004).
- [24] J. Cardy, in *Fields, strings and critical phenomena*, edited by E. Brezin and J. Zinn-Justin (Les Houches, 1988).
- [25] J.H. Wilkinson, in *The algebraic eigenvalue problem* (Oxford University Press, 1988).